

K-edge XANES of substitutional and interstitial Mn atoms in (Ga,Mn)As

N. A. Goncharuk, J. Kučera, K. Olejník, V. Novák, and L. Smrčka
*Institute of Physics, Academy of Sciences of the Czech Republic, v.v.i.,
Čukrovarnická 10, 162 53 Prague 6, Czech Republic*

Z. Matěj, L. Nichtová, and V. Holý
*Charles University, Faculty of Mathematics and Physics, Department of Condensed Matter Physics,
Ke Karlovu 5, 121 16 Prague 2, Czech Republic*

(Dated: May 6, 2019)

This work reports theoretical and experimental study of the X-ray absorption near-edge structure (XANES) at the Mn K-edge in (Ga,Mn)As diluted magnetic semiconductors. The spectra have been calculated from the first-principles using FLAPW including the core-hole effect, a special attention has been paid to consequences of coexistence of Mn impurities in substitutional and tetrahedral interstitial positions. We have performed quantitative component analysis of experimental spectra collected on the (Ga,Mn)As samples before/after annealing and etching, with the aim to determine the proportion of Mn impurity configurations. Comparison of the experimental data with theoretical computations indicates that even after annealing and etching some Mn atoms still reside in interstitial sites, although the concentration of interstitial defects has been reduced by annealing.

PACS numbers: 75.50.Pp, 81.05.Ea, 71.15.Mb, 71.20.Nr, 61.72.Vv, 61.10.Ht, 78.70.Dm

I. INTRODUCTION

Recently, the Mn-doped GaAs system has received considerable attention in view of its potential use in spintronic technology, as it combines both semiconducting/semimetallic and ferromagnetic properties in one physical system^{1,2}. The positions of Mn dopants play a decisive role in determining the magnetic properties of (Ga,Mn)As. There are three of them with a comparable energy³. The substitutional Mn atoms, $\text{Mn}_{\text{Ga}}^{\text{sub}}$, occupying Ga sites, act as hole-producing acceptors which contribute to ferromagnetism. The Mn atoms in tetrahedral interstitial positions, surrounded by either As or Ga atoms, $\text{Mn}_{\text{As}}^{\text{int}}$ and $\text{Mn}_{\text{Ga}}^{\text{int}}$, are electron-producing double donors which hinder ferromagnetic states. They partly compensate the Mn acceptors in the substitutional positions and reduce the number of holes that mediate ferromagnetism^{4,5}. Post-growth annealing of (Ga,Mn)As samples at low temperatures, close to the growth temperature, is known to improve magnetic properties of the (Ga,Mn)As system⁶⁻¹³. The concentration of Mn interstitials is reduced via out-diffusion through the hexagonal interstitial sites towards a surface where they oxidize. A Mn-rich oxide layer formed on the surface can be removed by etching¹⁴.

The X-ray absorption spectroscopy is the traditional tool which is used to characterize the local environment of impurities^{15,16}. Not long ago a few works have been published reporting on computations of XANES at the Mn K-edge in ternary (Ga,Mn)As alloys¹⁷⁻²¹ and in related diluted magnetic semiconductors²²⁻²⁵. However, most of these XANES studies concern mainly substitutional Mn defects. In the present paper a special attention is paid to interpretation of X-ray absorption spectra measured on Mn-doped GaAs materials in which different types of impurities coexist.

Let us note that recently detailed investigations focused on the configuration of substitutional and interstitial Mn impurities in (Ga,Mn)As have been performed with cross-sectional scanning tunneling microscopy (XSTM)²⁶ and electron paramagnetic resonance (EPR)²⁷.

Our study is based on the comparison of experimental XANES with spectra calculated by the method of full potential linearized augmented plane waves (FLAPW)²⁸. An isolated defect is represented by a supercell which should be as large as possible to describe correctly the absorption process. Therefore, we simulate the spectra from different types of defects by separated calculations, considering always only one substitutional or interstitial atom in a supercell.

If we consider an isolated Mn impurity, the position of the Fermi energy on the energy scale depends on the defect type, i.e., it is fixed by the acceptor level near the top of the valence band for the substitutional atom and by the donor levels close to the bottom of the conduction band for the interstitial atoms, respectively. The situation is similar in the supercell scheme with a single defect in each supercell. The concentration of defects is finite, the acceptor/donor levels are broadened and merge with the valence/conduction band, but the Fermi energy remains fixed near the valence or conduction band, depending on the defect type. This complicates the quantitative analysis of experimental absorption spectra on the basis of the linear combination of theoretical spectra calculated separately for each impurity.

In the real crystal with a mixture of defects the position of the Fermi energy is determined by the type of defects with the higher concentration, i.e., in the ferromagnetic (Ga,Mn)As by concentration of acceptors. We model this situation by replacing the Fermi energy of supercells with donors by the Fermi energy of the supercell

with an acceptor. This shift of the Fermi energy must be respected in the linear combination of spectra fitting of the experimental data.

II. EXPERIMENT

The measurements have been carried out at the European Synchrotron Radiation Facility in Grenoble, beamline BM29. The XANES spectra have been obtained by measuring the Mn K_α fluorescence as a function of the energy of incident photons around the energy of the Mn K absorption threshold, $E_o = 6539$ eV.

The measurements have been performed in the grazing-incidence mode, in which the penetration depth of the primary X-ray beam was sensitively tuned by changing the incidence angle α of the primary radiation in the range from 0.1° to 0.45° , i.e., around the critical angle $\alpha_c \approx 0.38^\circ$ of total external reflection. Increasing the incidence angle in this range, the penetration depth grows from few nanometers to several microns.

The fluorescence method of measurement was employed. The measured fluorescence signal comes from the transition of $2p$ L-shell core-level electrons to $1s$ K-shell core holes created by primary X-ray wave. The energy of the corresponding K_α fluorescence line is characteristic of the Mn atom and its intensity is proportional to the absorption coefficient (the XANES signal). Spectra were measured at room temperature.

The sample grown by molecular beam epitaxy (MBE) with $\sim 10.5 - 11\%$ of Mn content was used in our experiments. After annealing, the content of Mn was reduced to $\sim 7.5 - 8\%$. The annealed sample was etched in 35% HCl. Manganese K-edge XANES spectra were taken in fluorescence from the 42 nm thick sample of the as-grown, annealed and etched-after-annealing (Ga,Mn)As.

Two sets of experimental Mn K-edge XANES spectra, measured on the annealed and annealed-and-etched (Ga,Mn)As samples, are presented in Fig. 1 for various incidence angles α . The spectra can be separated into two parts: the pre-edge and main absorption. The pre-edge region, peaks A and B at around $E \sim 6540$ eV, lies below the steeply rising absorption edge, which culminates in the most intense post-edge peak C in the vicinity of $E \sim 6552 \div 6554$ eV, as illustrated in Fig. 1. All experimental spectra, including not presented here as-grown ones, exhibit the double structure (peaks A and B) separated by ~ 2.8 eV in the pre-edge absorption region.

In the annealed sample measured at lower α , the absorption edge grows almost linearly [Fig. 1a)]. With α increased, the spectra in this region acquire a convex shape and the position of the peak C moves to higher energies. The spectra taken at high α remind those measured on the annealed-and-etched sample [Fig. 1b)]. This spectrum modification must be due to removing the oxide layer from the sample surface by etching.

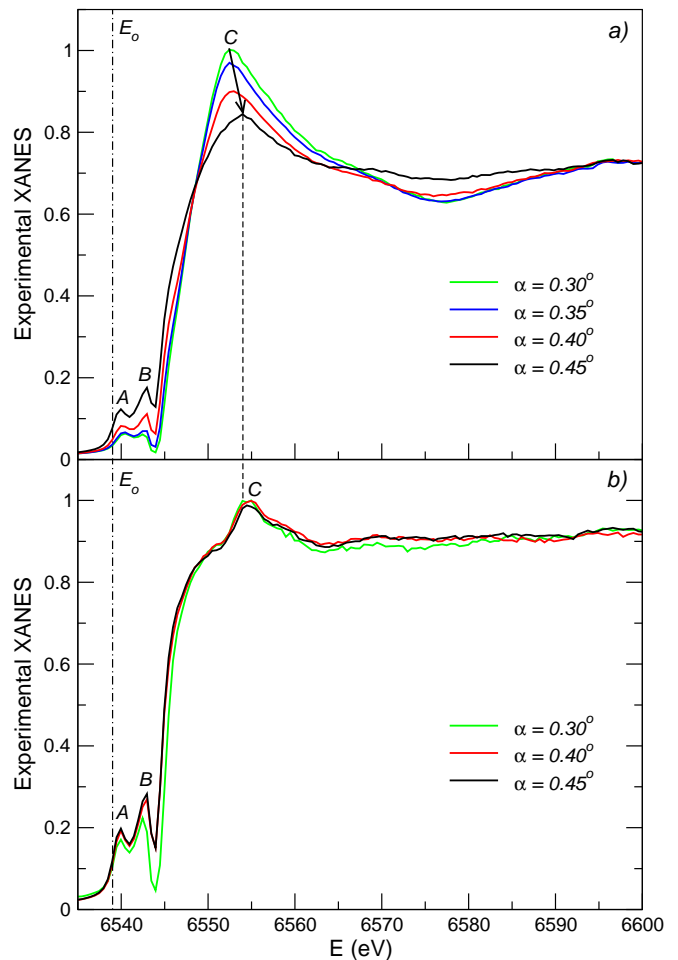


FIG. 1: (Color online) Experimental K-edge X-ray absorption spectra of Mn in (Ga,Mn)As measured at different incidence angles α of the primary X-ray beam. *a*) Spectra taken on the annealed sample with the Mn-rich surface oxide layer. *b*) Spectra taken on the annealed-and-etched sample without the Mn-rich surface oxide layer. All the spectra are normalized with respect to their high-energy ends. The different structures labeled A (pre-edge), B (pre-edge) and C (main absorption peak) are discussed in the text.

III. COMPUTATIONAL MODEL

The theoretical Mn K-edge XANES spectra and electronic band structures of (Ga,Mn)As were simulated using the full potential linearized augmented plane wave plus local orbitals (FLAPW + lo) method^{29,30} implemented by Blaha et al. in the WIEN2k package²⁸. A generalized gradient approximation (GGA)³¹ was employed for the exchange-correlation functional.

Basis wave functions were expanded in combinations of spherical harmonics inside non-overlapping muffin-tin (MT) spheres surrounding the atomic sites and in Fourier series in the interstitial region, with a cutoff of $R_{\text{MT}}K_{\text{max}}$ fixed at 7.0, where R_{MT} denotes the smallest MT sphere radius and K_{max} is the magnitude of the

largest k -vector in the plane wave expansion. The MT radii were assumed to be 1.29, 1.22 and 1.14 Å for Mn, Ga and As, respectively.

Brillouin zone integrations were performed using a tetragonal k -point mesh of Monkhorst-Pack type³⁴. Convergence of self-consistency was obtained using $5 \times 5 \times 5$ k -point sampling mesh in the reciprocal space of each supercell that corresponds to 10 k -points in the irreducible wedge of the Brillouin zone.

The spin-polarized calculations were performed within a 64-atom supercell based on the zinc-blende GaAs cubic cell with the experimental lattice constant $a = 5.65$ Å, doped with 3.125/3.03 atomic percent of Mn impurities in the substitutional/interstitial site. We always assumed a single Mn atom inside each supercell and used unrelaxed positions of the nearest neighbors around Mn. In the substitutional position the Mn atom is surrounded by 4 As with the unrelaxed Mn-As bond distance 2.445 Å, the second neighbors are 12 Ga on the distance 3.994 Å. When Mn is in one of interstitial positions, its first neighbors are either 4 As or 4 Ga, and the second neighbors are either 6 Ga or 6 As, respectively, with bond lengths equal to 2.445 Å and 2.822 Å. Thus, we expect that the difference between the energy structure in two configurations, $\text{Mn}_{\text{Ga}}^{\text{sub}}$ and $\text{Mn}_{\text{As}}^{\text{int}}$, in which Mn is surrounded by 4 As atoms is determined mainly by the second nearest neighbors.

The total density of states (DOS) calculated for three supercells are shown in the top three panels of Fig. 2 together with the DOS of GaAs and positions of the Fermi levels, which reflect the presence of either acceptor or donor impurities. As mentioned in Sec. I, the Fermi level in ferromagnetic (Ga,Mn)As is determined by prevalence of acceptors, and situated in the band composed of the merged valence and broadened acceptor impurity band. Consequently, we will consider the states above the $\text{Mn}_{\text{Ga}}^{\text{sub}}$ Fermi level as empty also for DOS calculated for $\text{Mn}_{\text{As}}^{\text{int}}$ and $\text{Mn}_{\text{Ga}}^{\text{int}}$ when interpreting XANES spectra.

We support this approach by calculation of the Fermi level positions in unrealistic 64-atom supercells with incorporated 4 $\text{Mn}_{\text{Ga}}^{\text{sub}}$ and 1 $\text{Mn}_{\text{As}}^{\text{int}}/\text{Ga}$. The results are shown in two bottom panels of Fig. 2. As expected, the resulting Fermi energies are shifted closer to the value obtained for the supercell with a single substitutional impurity.

In the single-electron approximation, which is used in our model, the absorption spectrum is given by a transition between the initial ground state with fully occupied core-levels and the final state with one core electron removed. The core-hole effect is known to be quite important for reproducing experimental spectra by theoretical calculations^{32,33}. Therefore, we repeated our self-consistent calculations also for excited states with one core electron removed from the Mn 1s level and an additional valence electron placed close to the bottom of the conduction band to fill the lowest unoccupied 4p orbital.

The energy of the absorbed radiation is determined as a difference between the calculated total energies of the

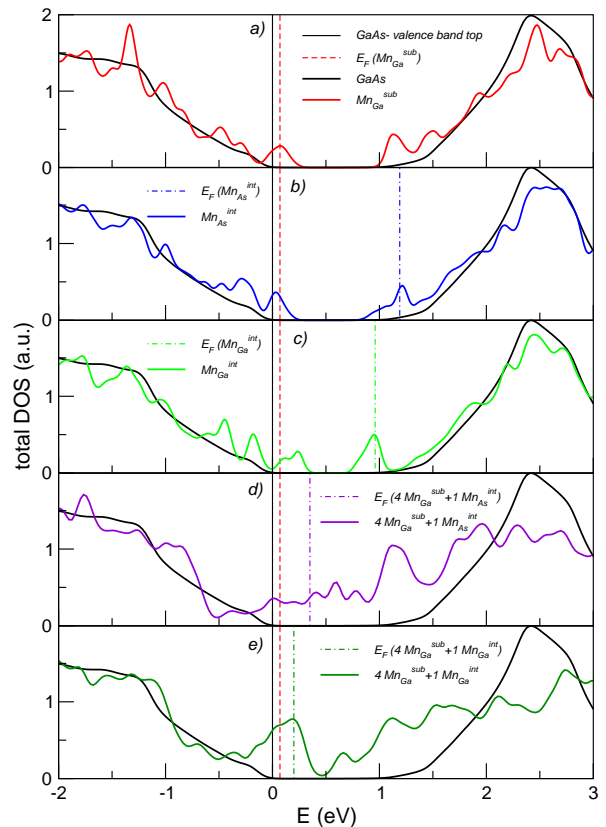


FIG. 2: The total DOS of GaAs (black curve) together with total DOSs of (Ga,Mn)As with embedded *a*) single substitutional Mn atom, *b*) single interstitial Mn atom inside the As tetrahedron, *c*) single interstitial Mn atom inside the Ga tetrahedron, *d*) cluster of four substitutional Mn atoms and one interstitial Mn atom inside the As tetrahedron, and *e*) cluster from four substitutional Mn atoms and one interstitial Mn atom inside the Ga tetrahedron. The full horizontal line at $E = 0$ eV denotes the top of the valence band. The Fermi energies of particular supercells are indicated by dashed vertical lines.

initial and final states. Note, that the influence of Mn 1s core-level shifts due to adjacent As or Ga atoms is included automatically in the self-consistent calculation. For the supercells with interstitial Mn atoms this energy must be further corrected by the Fermi level shifts, as mentioned above.

Due to the very small radius of Mn 1s K-shell core hole the absorption spectrum is given as a product of the transition probability, calculated from 1s - 4p dipole matrix elements, which is a smooth function of energy, and the local partial DOS of 4p-states above the Fermi energy in the MT sphere surrounding the Mn atom, obtained from the final state calculation.

IV. DATA ANALYSIS AND RESULTS

A. First-principles XANES simulations

The simulated XANES Mn K-edge spectra for three types of isolated Mn defects are reported in Fig. 3. All curves were normalized and convoluted with a Lorentz function modeling the experimentally induced broadening. A parameter of a full width at half maximum (FWHM) $\gamma = 1$ eV was chosen for a fair comparison between experimental and calculated spectra. The use of the broadening with larger γ would mask the fine details of theoretical curves in the pre-edge region.

The transition energy was obtained by a difference in total electronic energies between the ground and core-hole states. The theoretical transition energy deviates from the experimental one (threshold, $E_o = 6539$ eV) by -22 eV ($|\Delta E/E| = 0.336\%$), which is reflected in Fig. 3 by the corresponding shift of the energy scale.

Similarly to the experimental XANES spectra, the pre-edge and main absorption parts can be distinguished.

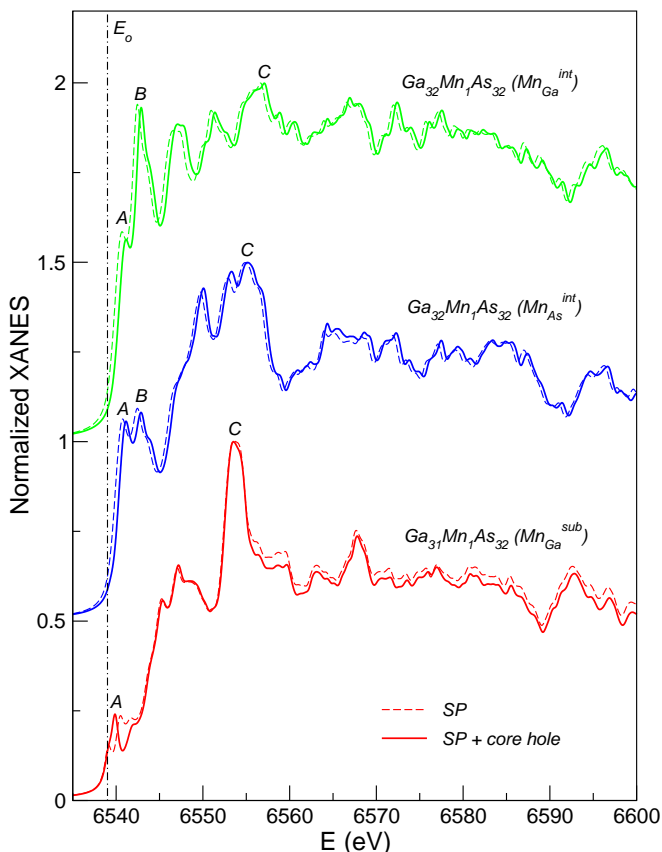


FIG. 3: Normalized ab-initio K-edge XANES spectra of Mn in the 64-atom (Ga,Mn)As supercell simulated for three different Mn sites in the substitutional (Mn_{Ga}^{sub}) and two tetrahedral interstition positions (Mn_{As}^{int} and Mn_{Ga}^{int}). Solid/dashed curves are spin-polarized spectra calculated with/without the core-hole effect.

An intense double structure (peaks A and B) appears in the pre-edge region for both types of interstitial defects, Mn_{As}^{int} and Mn_{Ga}^{int} , in contrast to a weak single peak A for a substitutional Mn impurity, Mn_{Ga}^{sub} .

Arrangement of neighboring atoms around the absorbing Mn atom strongly affects the pre-edge structure. The intensity of pre-edge peaks is much larger for interstitials compared to that for the substitutional model spectrum. In accordance with Wong³⁵, we attribute this difference to the different distance of the second neighbor shell ligands from the X-ray absorbing Mn centers. As already mentioned in Sec. III, all considered Mn impurities are located inside tetrahedrons composed of As/Ga atoms with the same bond length of the first neighbor shell ligands. However, the bond distance of the second nearest neighbor ligands of interstitials is by 1.172 Å less than that of Mn_{Ga}^{sub} . In the Wong’s terminology, the smaller the “molecular cage”, the higher the intensity of the pre-edge absorption.

As for the core-hole influence on the shape of the calculated spectra, our results imply that it is significant only in the pre-edge region of the substitutional Mn defect and is not important in the main part of absorption curves. With the core-hole effect introduced, the spectral structure of both type of interstitials was only shifted by -0.4 eV but its shape remained the same. Let us now discuss the pre-edge electronic structure in more detail.

The band structure of (Ga,Mn)As with Mn_{Ga}^{sub} calculated without/with taking into account the core-hole effect is shown in Figs. 4,5. When Mn atom is in the substitutional position it is surrounded by four As atoms located on the vertices of a tetrahedron. The tetrahedral crystal field of As ions splits $3d$ -states of Mn into e_g - and t_{2g} -levels with e_g below t_{2g} ^{36–38}. Exchange interactions further split these states into spin-up (\uparrow) and spin-down (\downarrow) states. Due to the tetrahedral arrangement the t_{2g} -states of the Mn atom hybridize with Mn $4p$ -states. The states resulting from hybridization of the deeper t_{2g}^{\uparrow} -states have mainly Mn d character, while those resulting from higher t_{2g}^{\downarrow} -states have dominantly As p character. In contrast, e_g -levels of Mn have no states available for significant coupling since the GaAs host does not have e_g -states localized in this energy range. It is seen in Fig. 4 that the density of Mn p -states is larger at the energy of $d_{t_{2g}}$ -states in comparison with that at the energy of d_{e_g} -states.

It is obvious from the discussion above that the pre-edge fine structure of Mn K-edge XANES with Mn_{Ga}^{sub} originates from the transfer of $1s$ electrons to valence $3d$ states mediated by $1s-4p$ dipole transition and $4p-3d$ hybridization. We observed two weak absorption lines corresponding to $1s-t_{2g}^{\uparrow}$ and $1s-t_{2g}^{\downarrow}$ electron transfers in the absorption spectrum calculated without the core-hole correction [see Fig. 4 c)]. The first transfer is only partly available as the Fermi level touches the t_{2g}^{\uparrow} -band near its border, leaving a little amount of empty t_{2g}^{\uparrow} -states. After

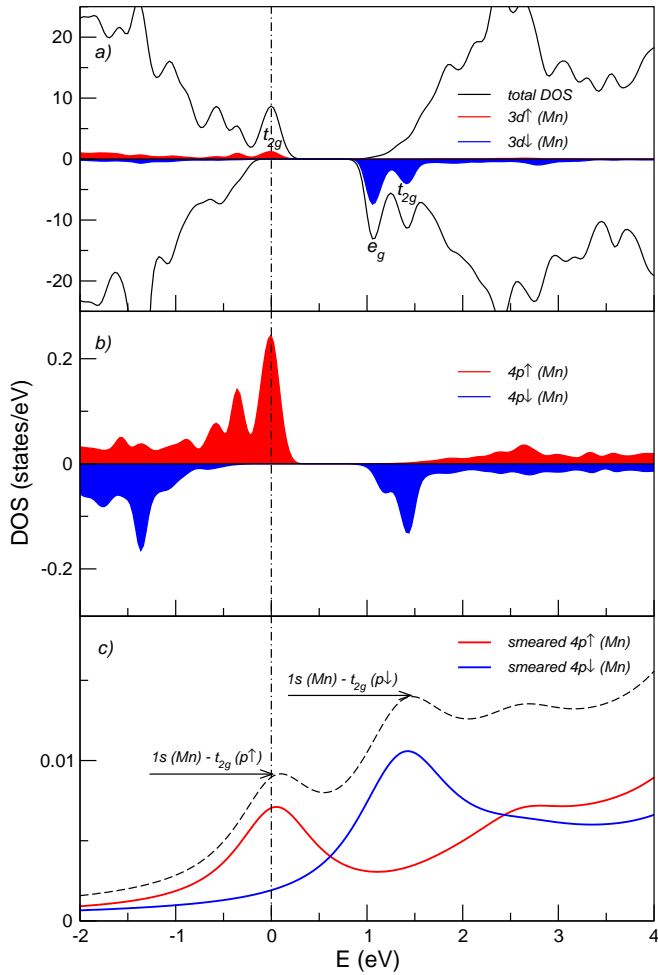


FIG. 4: (Color online) The total and partial DOSs in the $\text{Ga}_{31}\text{Mn}_1\text{As}_{32}$ supercell with a Mn atom in the substitutional site calculated without the core-hole effect. *a)* The total DOSs (solid curves) and densities of Mn $3d$ -states (filled regions). *b)* The density of $4p$ -states of Mn. *c)* The smeared density of $4p$ -states of Mn (the X-ray absorption spectrum divided by the corresponding matrix element). The majority/minority spin DOSs are shown in the upper/lower part of figures. The vertical dash-dot line denotes the Fermi level. The electron transitions in the pre-edge part of the absorption spectrum are depicted by arrows.

introduction of the core-hole effect, two aforementioned lines join into one line of higher intensity [see Fig. 5 *c)*], and the transfer $1s-t_{2g}^{\downarrow}$ became dominant. In this case the Mn t_{2g}^{\uparrow} -states are fully filled with electrons and the transfer $1s-t_{2g}^{\uparrow}$ becomes impossible.

The band structures of $(\text{Ga},\text{Mn})\text{As}$ calculated with incorporated interstitials $\text{Mn}_{\text{As}}^{\text{int}}$ and $\text{Mn}_{\text{Ga}}^{\text{int}}$, and taking into account the core-hole effect, are shown in Figs. 6,7. For both interstitials, we observe two intense pre-edge absorption lines A and B, which are originated from the $1s-4p$ transitions. This is in contrast to the pre-edge structure of $\text{Mn}_{\text{Ga}}^{\text{sub}}$. Both peaks are mainly of dipolar

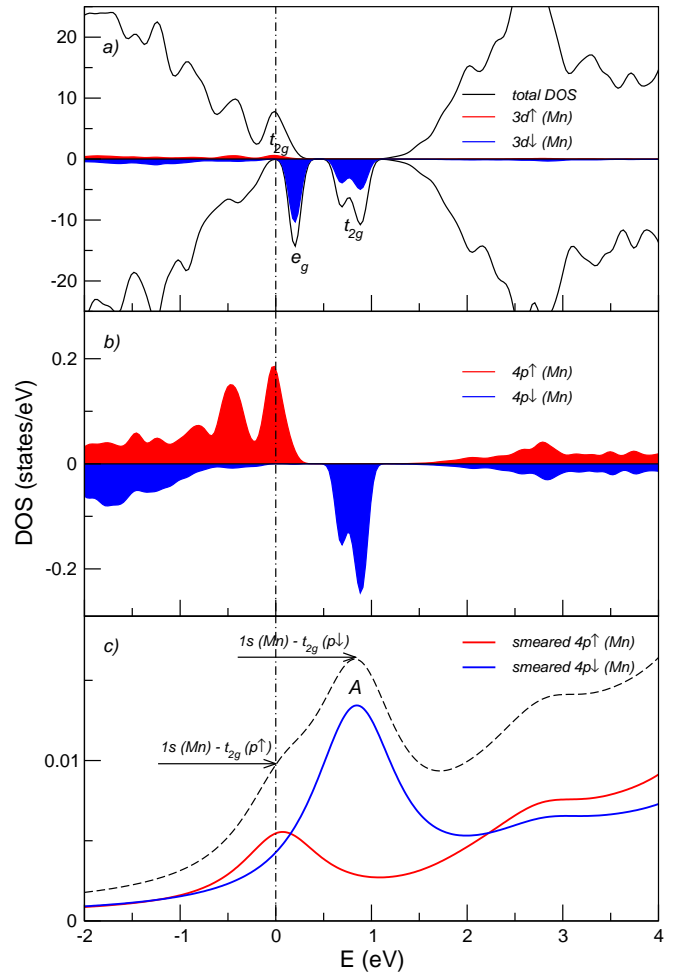


FIG. 5: (Color online) The same as in Fig. 4 calculated with the core-hole effect.

origin. The Fermi level separates occupied and unoccupied states. In the case of interstitial impurities it is fixed in the band composed of the merged conduction and broadened donor impurity band. The Fermi level falls in the t_{2g}^{\uparrow} -band for $\text{Mn}_{\text{As}}^{\text{int}}$ and t_{2g}^{\downarrow} -band for $\text{Mn}_{\text{Ga}}^{\text{int}}$. However, these two bands do not contribute to the pre-edge absorption structure due to low density of Mn $3d$ -states near the Fermi level. In contrast to the case with the substitutional Mn, the $t_{2g}^{\uparrow}/t_{2g}^{\downarrow}$ -states near the Fermi level do not participate in $4p-3d$ hybridization. Thus, both peaks are mainly of dipolar origin, and their shape replicates the DOS of Mn $4p$ -states.

B. Experiment versus theory

As already demonstrated in Sec. II, all experimental spectra (as-grown, annealed, and annealed-and-etched) have got the double structure in the pre-edge absorption. In Sec. IV A we showed that all examined Mn impurities can contribute to the first pre-edge peak A. Only Mn in-

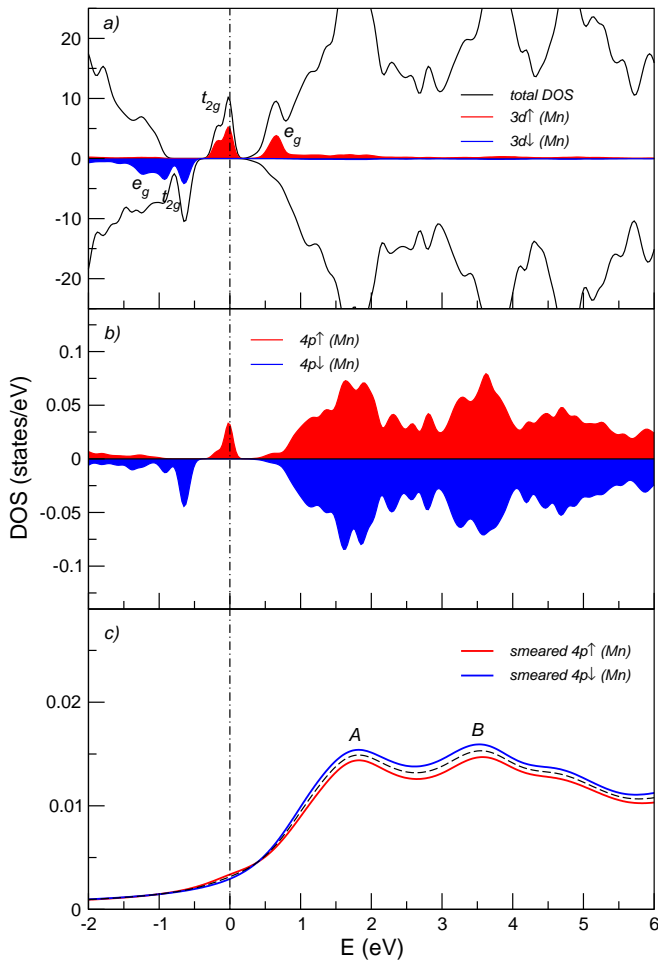


FIG. 6: (Color online) The same as in Fig. 4 for the $\text{Ga}_{32}\text{Mn}_1\text{As}_{32}$ supercell with the interstitial Mn atom inside the As tetrahedron calculated with the core-hole effect.

terstitials are responsible for the intensity growth of the second pre-edge peak B. It implies that at least small proportion of interstitial Mn defects is present in the compound. The intensity ratios of experimental peaks B and A differs for different incidence angles of the X-ray radiation, α . The tendency of B/A variation deep inside the sample is displayed in Fig. 8. Close to the surface, $\alpha = 0.3^\circ$, the ratio B/A, i.e., the content of Mn atoms in interstitial positions, is smaller in the as-grown and annealed samples, compare to the etched one. It is believed that the as-grown and annealed samples have a thick layer of Mn oxide on the surface, and the penetration depth of the X-ray beam inside the sample is small at small α , as it is reduced by the width of the oxide layer. In the annealed-and-etched sample the ratio B/A grows slowly with α . Thus, the Mn defect distribution is almost depth independent. The content of Mn impurities becomes equal in both annealed and etched samples at large $\alpha = 0.45^\circ$ deep inside the sample where the oxid layer is of no importance.

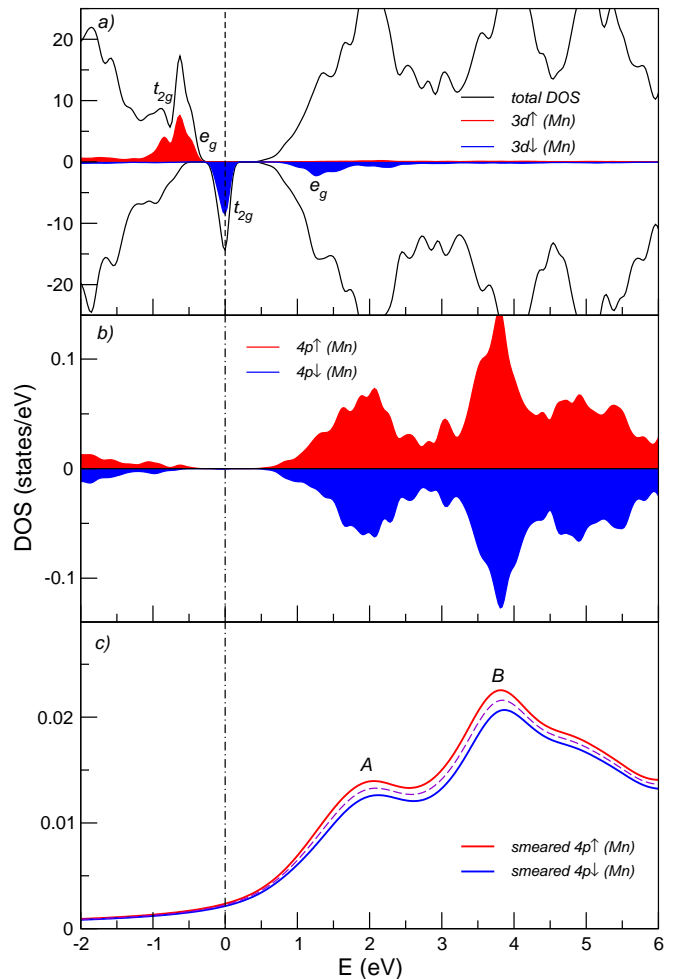


FIG. 7: (Color online) The same as in Fig. 4 for the $\text{Ga}_{32}\text{Mn}_1\text{As}_{32}$ supercell with the interstitial Mn atom inside the Ga tetrahedron with the core-hole effect.

The simulated data have been processed to explain the experimental XANES spectra. Our aim was to guess a rough number of Mn impurities that can reproduce the experimental spectra. Results are present in Figs. 9,10.

Before performing a fit we fixed the Fermi energy of the supercell with embedded substitutional Mn atom, $E_F(\text{Mn}_{\text{Ga}}^{\text{sub}}) = 4.609$ eV. The absorption spectra obtained for Mn interstitials were shifted relative to the spectrum calculated for the substitutional Mn by $\Delta E_F = E_F(\text{Mn}_{\text{Ga}}^{\text{sub}}) - E_F(\text{Mn}_{\text{As/Ga}}^{\text{int}})$, which is -0.831 eV (for $\text{Mn}_{\text{As}}^{\text{int}}$) and -0.578 eV (for $\text{Mn}_{\text{Ga}}^{\text{int}}$), correspondingly.

We found that the content of $\text{Mn}_{\text{Ga}}^{\text{sub}}$ prevails over the content of both interstitial impurities, especially deep inside the sample ($\alpha \geq 0.40^\circ$). We have got 83% of $\text{Mn}_{\text{Ga}}^{\text{sub}}$ and 17% of interstitials. The intensity of the peak B can be changed by the variation of the proportion of $\text{Mn}_{\text{As}}^{\text{int}}$ and $\text{Mn}_{\text{Ga}}^{\text{int}}$. The more $\text{Mn}_{\text{Ga}}^{\text{int}}$, the higher the feature B. Analogously to the experimental curve, the theoretical fit has a convex shoulder above the absorption edge, which has been observed only on the annealed-and-etched sam-

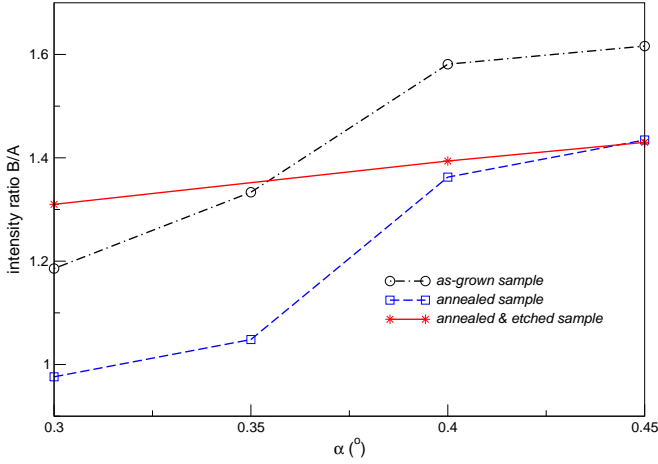


FIG. 8: The ratio of experimental pre-edge peak intensities B and A, obtained from measurements on the as-grown, annealed and annealed-and-etched sample as a function of the incidence angle α of the primary X-ray radiation.

ple [Fig. 1 b)].

Our fit is not exact which indicates shortages of the component analysis method. The separation of experimental pre-edge peaks A and B is larger by ~ 0.8 eV in comparison with the distance obtained theoretically. We explain it by the fact that the theoretical width of the energy band gap of the GaAs host material is smaller than the experimental width.

Experimental data obtained for the non-etched annealed sample show an increase in the intensity ratio

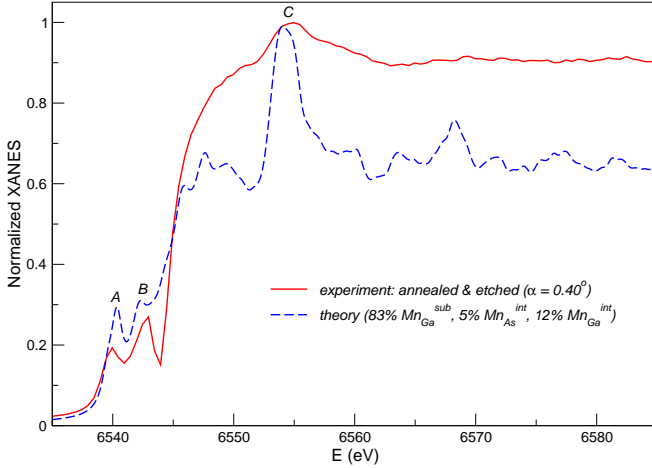


FIG. 9: Comparison of the normalized experimental and theoretical K-edge XANES spectra of Mn in (Ga,Mn)As. The experimental spectrum (solid curve) was measured on the annealed-and-etched sample without the Mn-rich surface oxide layer at $\alpha = 0.40^\circ$. The theoretical spectrum (dashed curve) is obtained by a linear combination of the model XANES spectra calculated for $\text{Mn}_{\text{Ga}}^{\text{sub}}$, $\text{Mn}_{\text{As}}^{\text{int}}$ and $\text{Mn}_{\text{Ga}}^{\text{int}}$ site defects.

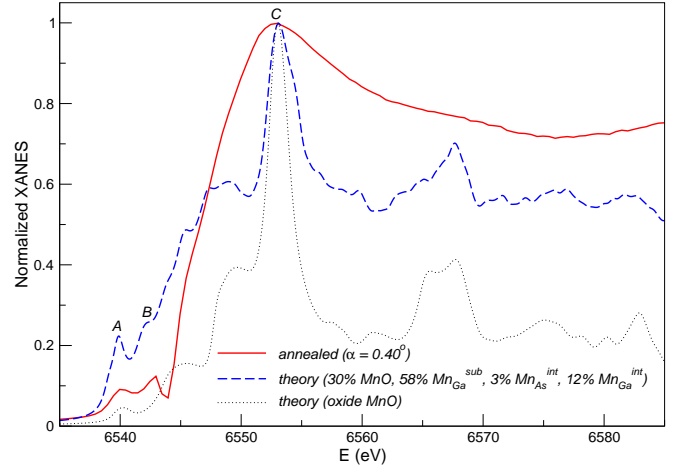


FIG. 10: Comparison of the normalized experimental and theoretical K-edge XANES spectra of Mn in (Ga,Mn)As. The experimental spectrum (solid curve) was measured on the annealed sample with the Mn-rich surface oxide layer at $\alpha = 0.40^\circ$. The theoretical spectrum (dashed curve) is obtained by a linear combination of the model XANES spectra calculated for $\text{Mn}_{\text{Ga}}^{\text{sub}}$, $\text{Mn}_{\text{As}}^{\text{int}}$, $\text{Mn}_{\text{Ga}}^{\text{int}}$ site defects and MnO oxide. The latter spectrum is shown (dotted curve).

between the highest peak C and lowest peaks A, B in comparison with the etched sample (Fig. 10). The shoulder above the absorption edge is observed only for high α , the main peak C becomes sharper. Such phenomenon can be explained by combined influence of both the content changes of Mn defects in (Ga,Mn)As and the presence of the oxide layer on the sample surface. To illustrate our assumption, we add an additional component, the Mn K-edge XANES spectrum of MnO oxide, to the linear combination of three Mn model spectra in (Ga,Mn)As, and plotted the fit together with the experimental curve, as depicted in Fig. 10. The main peak C in the fit becomes sharper, the shoulder smooths, and the intensity ratio between the main and pre-edge structures reduces at the expense of the Mn oxide component

V. CONCLUSION

We have performed an extensive LAPW numerical study of K-edge XANES spectra of the substitutional and two tetrahedral interstitial Mn sites in (Ga,Mn)As supercells. We have found out that the effect of the core hole is essential for $\text{Mn}_{\text{Ga}}^{\text{sub}}$. We studied the whole range of absorption spectra, the highest intensity Mn absorption lines in the main part of XANES above the absorption edge and weak lines in the pre-edge part of XANES where the sharp distinction between the spectra with substitutional and interstitial Mn defects has been observed. The difference between simulated spectra is determined mainly by the second nearest neighbor ligands. Two peaks appear in the pre-edge region for any inter-

stitial defect, whereas a smaller single peak is obtained for a substitutional Mn impurity. All pre-edge peaks are small in intensity in comparison with the corresponding highest peak C in the main part. The combination of theoretical spectra for various contents of Mn atoms in both substitutional and interstitial positions gives a reasonable qualitative fit of experimental data collected on the annealed and etched sample. Summarizing the experimental and theoretical evidence, we have revealed that even after annealing and etching of our sample some Mn atoms still reside in interstitial sites, as spectra with two small peaks are always observed experimentally.

VI. ACKNOWLEDGEMENTS

The assistance of Dr. S. Pascarelli from the beamline BM28 at ESRF Grenoble is highly appreciated. This work has been supported by the Ministry of Education of the Czech Republic (Center for Fundamental Research LC510 and the research program MSM0021620834), and Academy of Sciences of the Czech Republic project KAN400100652.

-
- ¹ Y. Ohno, D. K. Young, B. Beschoten, F. Matsukura, H. Ohno, D. D. Awschalom, *Nature* **402**, 790 (1999).
 - ² H. Ohno, D. Chiba, F. Matsukura, T. Omiya, E. Abe, T. Dietl, Y. Ohno, K. Ohtani, *Nature* **408**, 944 (2000).
 - ³ J. Mašek, F. Máca, *Phys. Rev. B* **69**, 165212 (2004).
 - ⁴ T. Jungwirth, J. Sinova, J. Mašek, J. Kučera, A. H. MacDonald, *Theory of ferromagnetic (III,Mn)V semiconductors*, *Rev. Mod. Phys.* **78**, 809 (2006).
 - ⁵ J. Sinova, T. Jungwirth, J. Černe, *Int. J. of Modern Phys.* **18**, 8, 1083 (2004).
 - ⁶ K. M. Yu, W. Walukiewicz, T. Wojtowicz, L. Kuryliszyn, X. Liu, Y. Sasaki, J. K. Furdyna, *Phys. Rev. B* **65**, 201303 (2002).
 - ⁷ K. W. Edmonds, K. Y. Wang, R. P. Champion, A. C. Neumann, N. R. S. Farley, B. L. Gallagher, C. T. Foxon, *Appl. Phys. Lett.* **81**, 4991 (2002).
 - ⁸ Y. Hashimoto, T. Hayashi, S. Katsumoto, Y. Iye, *J. Cryst. Growth* **237**, 1334 (2002).
 - ⁹ I. Kuryliszyn, T. Wojtowicz, X. Liu, J. K. Furdyna, W. Dobrowolski, J. -M. Broto, O. Portugall, H. Rakoto, B. Raquet, *J. Supercond.* **16**, 63 (2003).
 - ¹⁰ D. Chiba, K. Takamura, F. Matsukura, H. Ohno, *Appl. Phys. Lett.* **82**, 3020 (2003).
 - ¹¹ M. B. Stone, K. C. Ku, S. J. Potashnik, B. L. Sheu, N. Samarth, P. Schiffer, *Appl. Phys. Lett.* **83**, 4568 (2003).
 - ¹² W. Limmer, A. Koeder, S. Frank, M. Glunk, W. Schoch, V. Avrutin, K. Zuern, R. Sauer, A. Waag, *Physica E* **21**, 970 (2003).
 - ¹³ K. W. Edmonds, P. Boguslawski, K. Y. Wang, R. P. Champion, S. N. Novikov, N. R. S. Farley, B. L. Gallagher, C. T. Foxon, M. Sawicki, T. Dietl, M. B. Nardelli, J. Bernholc, *Phys. Rev. Lett.* **92**, 037201 (2004).
 - ¹⁴ K. Olejník, M. H. S. Owen, V. Novák, J. Mašek, A. C. Irvine, J. Wunderlich, T. Jungwirth, *Phys. Rev. B* **78**, 054403 (2008).
 - ¹⁵ *X-Ray Absorption: Principles, Applications, Techniques of EXAFS, SEXAFS and XANES*, edited by D. C. Koningsberger and R. Prins, John Wiley (1998).
 - ¹⁶ *Elements of Modern X-Ray Physics*, edited by J. Als-Nielsen and D. McMorrow, John Wiley (2001).
 - ¹⁷ R. Bacewicz, A. Twaróg, A. Malinowska, T. Wojtowicz, X. Liu, J. K. Furdyna, *J. of Phys. and Chem. of Solids* **66**, 2004 (2005).
 - ¹⁸ A. Titov, X. Biquard, D. Halley, S. Kuroda, E. Bellet-Amalric, H. Mariette, J. Cibert, A. E. Merad, G. Merad, M. B. Kanoun, E. Kulatov, Yu. A. Uspenskii, *Phys. Rev. B* **72**, 115209 (2005).
 - ¹⁹ A. Titov, E. Kulatov, Yu. A. Uspenskii, X. Biquard, D. Halley, S. Kuroda, E. Bellet-Amalric, H. Mariette, J. Cibert, *Journal of Magnetism and Magnetic Materials* **300**, 144 (2006).
 - ²⁰ F. d'Acapito, G. Smolentsev, F. Boscherini, M. Piccin, G. Bais, S. Rubini, F. Martelli, A. Franciosi, *Phys. Rev. B* **73**, 035314 (2006).
 - ²¹ A. Wolska, K. Lawniczak-Jablonska, M. T. Klepka, R. Jakiela, J. Sadowski, I. N. Demchenko, E. Holub-Krappe, A. Persson, D. Arvanitis, *Acta Physica Polonica A* **114**, 357 (2008).
 - ²² X. Biquard, O. Proux, J. Cibert, D. Ferrand, H. Mariette, R. Giraud, B. Barbara, *J. Superconductivity* **16**, 127 (2003).
 - ²³ S. Sonoda, Y. Yamamoto, T. Sasaki, K. Suga, K. Kindo, H. Hori, *Solid State Commun.* **133**, 177 (2005).
 - ²⁴ O. Sancho-Juan, A. Cantarero, G. Martínez-Criado, N. Garro, A. Cros, M. Salomé, J. Susini, S. Dhar, K. Ploog, *Phys. Stat. Sol. B* **243**, 1692 (2006).
 - ²⁵ S. Wei, W. Yan, Z. Sun, Q. Liu, W. Zhong, X. Zhang, H. Oyanagi, Z. Wu, *Appl. Phys. Lett.* **89**, 121901 (2006).
 - ²⁶ A. Stroppa, X. Duan, M. Peressi, D. Furlanetto, S. Modesti, *Phys. Rev. B* **75**, 195335 (2007).
 - ²⁷ T. Weiers, *Phys. Rev. B* **73**, 033201 (2006).
 - ²⁸ P. Blaha, K. Schwarz, G. K. H. Madsen, D. Kvasnicka, J. Luitz, WIEN2k, *An Augmented Plane Wave plus Local Orbitals program for calculating crystal properties*, edited by K. Schwarz (Techn. Univ. Wien, Austria, 2007, ISBN 3-9501031-1-2).
 - ²⁹ K. Schwarz, A. Neckel, J. Nordgen, *J. Phys. F* **9**, 2509 (1979).
 - ³⁰ K. Schwarz, E. Wimmer, *J. Phys. F* **10**, 1001 (1980).
 - ³¹ J. P. Perdew, K. Burke, M. Ernzerhof, *Phys. Rev. Lett.* **77**, 3865 (1996).
 - ³² T. Yamamoto, T. Mizoguchi, I. Tanaka, *Phys. Rev. B* **71**, 245113 (2005).
 - ³³ S. Nakashima, K. Fujita, K. Tanaka, K. Hirao, T. Yamamoto, I. Tanaka, *Phys. Rev. B* **75**, 174443 (2007).
 - ³⁴ H. J. Monkhorst, J. D. Pack, *Phys. Rev. B* **13**, 5188 (1976).
 - ³⁵ J. Wong, F. W. Lytle, R. P. Messmer, D. H. Maylotte, *Phys. Rev. B* **30**, 5596 (1984).
 - ³⁶ P. Mahadevan, A. Zunger, *Phys. Rev. B* **68**, 075202 (2003).
 - ³⁷ K. Sato, H. Katayama-Yoshida, *Semicond. Sci. Technol.* **17**, 367 (2002).
 - ³⁸ P. Mahadevan, A. Zunger, *Phys. Rev. B* **69**, 115211 (2004).